applied mechanics

MDPI

Article

Flow-Based Anatomy of Bobbin Friction-Stirred Weld; AA6082-T6 Aluminium Plate and Analogue Plasticine Model

Abbas Tamadon *, Dirk J. Pons * and Don Clucas

Department of Mechanical Engineering, University of Canterbury, Christchurch 8140, New Zealand; don.clucas@canterbury.ac.nz

* Correspondence: abbas.tamadon@pg.canterbury.ac.nz (A.T.); dirk.pons@canterbury.ac.nz (D.J.P.)

Received: 30 November 2019; Accepted: 17 January 2020; Published: 20 January 2020; Corrected: 5 March 2024

Abstract: Material flow transportation around the rotating tool and the mass deposition at the backside of the tool are critical characteristics of friction stir welding. To achieve an optimized weld structure, the history of the plastic deformation needs to be identified with a flow-based elucidation. In this study, an analogue model was applied to evaluate the formation of a banded structure using the bobbin tool, with a focus on the interaction between the tool-workpiece. The flow visualization in plasticine analogue was validated in comparison with the aluminium welds. The plastic flow mechanism was visualized both, at the surface and the cross-section of the weld-seam. The cross-section of the weld shows the details of the formation of tunnel voids, caused by the failure of the flow regimes. A physical model of the material flow was proposed to explain the formation mechanism of the tunnel void as a discontinuity during the mass refilling at the rear of the tool.

Keywords: bobbin friction stir welding; aluminium; analogue model; plastic deformation; material flow; tunnel void defect

1. Introduction

The bobbin-tool with a double-sided configuration [1–3] is an innovative tool variant for friction stir welding (FSW), suitable for solid-phase joining of aluminium alloys [4,5]. By modification of the FSW tool, bobbin friction stir welding (BFSW) has significant advantages in the production of butt-joint welds through the asymmetrical cross-section [3,6,7]. The double rotating shoulders in bobbin-tool can generate more heat compared to the single-shoulder conventional-FSW (CFSW) tool with a stationary backing anvil acting as a heat sink [8]. This enables the BFSW process to weld different thickness of workpiece with a simple process setup, in a shorter processing time/speed [8,9]. Recently, the significant potential of the BFSW has been applied for processing of high-strength aluminium alloys, e.g., 6xxx-series, which suffer from poor weldability [3,10]. However, this is a new technique which produces excellent joints without the presence of defects, and requires extensive investigation to identify the optimum welding parameters [11,12]. Since there is no solid theory about the details of the BFSW mechanism, this is also the subject of recent research to identify the role of the process variables affecting the weld properties [11–14].

In general, there is an agreement that the tool components (top and bottom shoulders and centred pin) are responsible for a significant portion of the friction action and subsequent heat generation [1,9,15]. By advancing the rotating tool through the initial butting interface position, the continuous plastic deformation and mixing of the material flow regimes from both sides of the tool (advancing side and retreating side) form solid-phase joining at the position of the stirring zone [16–18], see Figure 1. The welding process parameters (rotational and transverse speeds) and the tool geometry (thread, flat,

scroll) are mainly responsible for the heat input and formation of the stirring-based flow regimes, rather than metallurgical procedures during the interaction between the tool and the workpiece [15].

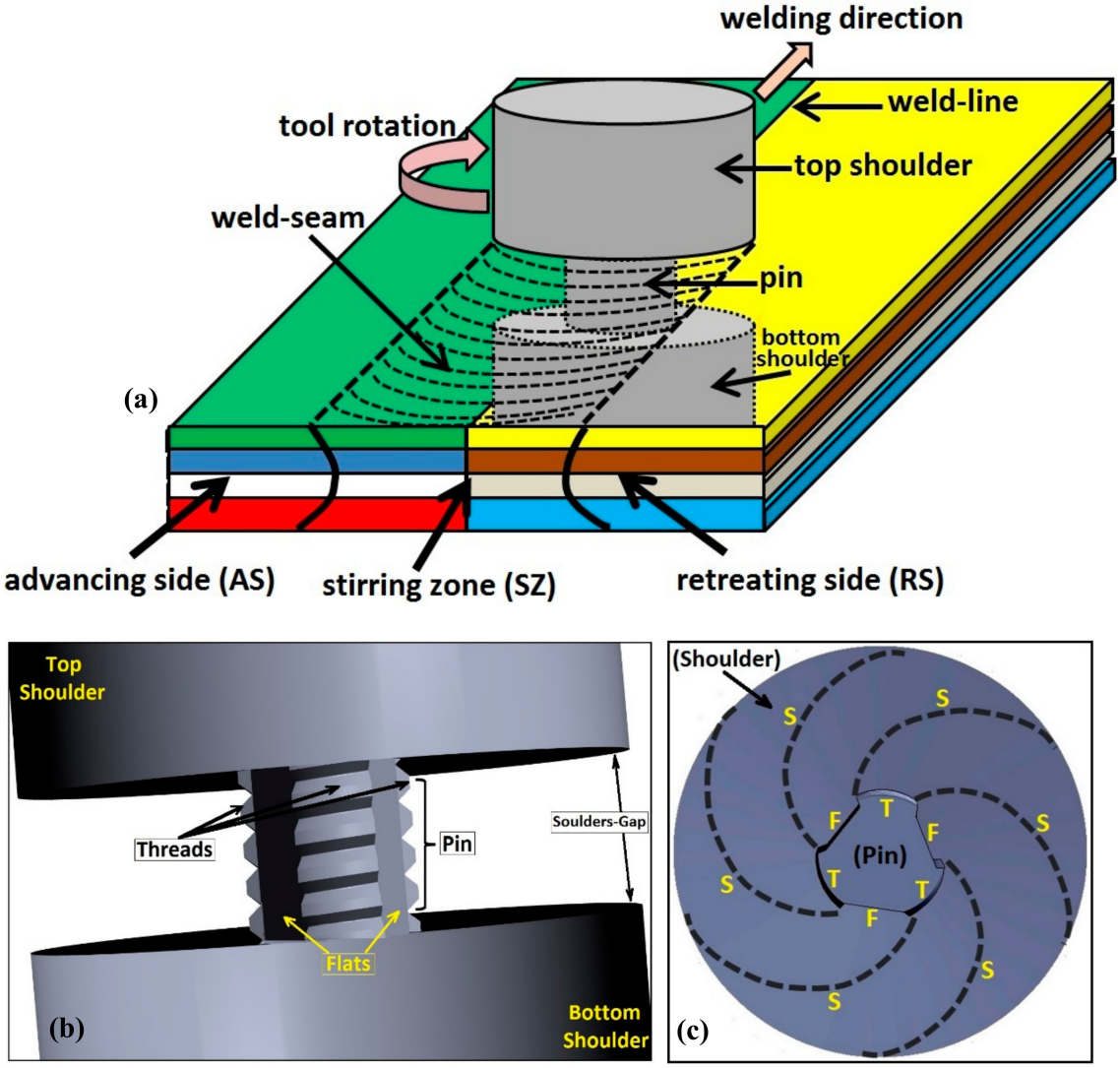

Figure 1. Schematic of the bobbin friction stir process; (**a**) interaction between the bobbin tool and the substrate (multi-layered plasticine slab), with details of the weld structure, (**b**) Three-dimensional (3D) model of the fully-featured bobbin-tool, (**c**) cross-section view of the bobbin-tool; position of the centred tri-flat pin and the scroll patterns on the shoulder surface, (F: flats, T: threads, S: scrolls).

Additionally, microstructural observation indicates the existence of some discontinuity defects (e.g., voids or crack) within the weld structure, which can severely deteriorate the mechanical properties of the weldment [19,20]. These defects can emerge because of the welding parameters or inaccuracy in control of the operation setup. Thus, insufficient heat input, or poor engagement of the tool-substrate may result in the failure of the flow regimes during stirring action [8,9]. Subsequently, unsuitable interaction of the operating variables reduces the required homogeneity in plastic deformation, resulting in the formation of physical defects within the structure of the welded joints [21].

Characterization of the flow-based details of the weld structure can indicate the quality of the weld in correlation to the welding variables [1,12,14]. In a general flow mechanism [22] in FSW, the formation of the joint requires a level of deformation and mixing of the material from both sides of the interface [11]. The dynamic interaction between the rotating tool and the substrate is poorly understood. The material flow through the weld transfers material from the leading edge of the tool

to the trailing edge around the pin [1]. This flow mechanism, while not completely understood, is evidently a key determinant of weld quality [23,24].

Flow visualization seeks to explain the plastic flow mechanism near the position of the tool. However, the demonstration of the actual flow pattern in the FSW process is difficult. The complex interaction between the rotating tool and the abutting base metal results in chaotic flow [25]. This can interfere with the identification of the actual flow mechanism and can result in the misinterpretation of the banded shear structures in the form of plastic flow lines [26].

For weld samples, the common etching technique is to visualise flow mixing with suitable contrast [20]. However, visualizing the shear bands is dependent on the response of the metal to the etchant reagent, which is difficult to achieve for some of the aluminium grades, e.g., 6xxx-series though that series has recently been solved [20]. Metallographic methods are laborious and any problems cause time costs in research. Therefore, there is value in developing new methods of material flow visualization that provide good contrast within the flow patterns.

Among various flow visualising techniques, the plasticine analogue has a suitable similarity to the etching results, in order to produce a physical model for the weld structure [12]. Plasticine analogue is an easily-prepared sample for visualizing metal forming processes generally, and for showing the detailed patterns of plastic deformation behaviour [11]. The contrast between the coloured layers of the plasticine can demonstrate the slip-lines patterns, which are representative of the shear bands in the flow fields of the material in the plasticity region [13]. Nevertheless, because of the inherent differences between the metallic structure, the accuracy of the produced flow patterns in plasticine analogue needs to be validated by comparing with the actual weld samples [14].

This work studies the anatomy of the BFSW weld structure with a focus on the flow features responsible for the formation of the defects within the plasticized weld material in their interaction with the bobbin-tool. The mixing behaviour of the material flow lines in the stirring zone is visualized by an innovative plasticizing flow model using plasticine analogue.

The plasticine analogue model was set up to replicate the results from a set of AA6082-T6 BFSW welding trials. The metallographic observations of the aluminium were consistent with the optical inspection of the plasticine samples, but the plasticine had more details about the flow mechanism during the tool-substrate interaction. Based on the flow visualization, the authors propose a physical model for the formation of the tunnel void, which is attributed to the flow-based origins of the weld failure.

2. Materials and Methods

For both plasticine analogue tests and actual aluminium welds, a full-featured fixed-gap bobbin tool was used, see Figure 1. Two set of tools were fabricated for the welding experiments, while the geometrical features were the same; two symmetrical scrolled shoulders at top and bottom and a tri-flat threaded pin in the middle. For the aluminium welding trials the bobbin-tool was made of H13 tool steel, and for processing the plasticine analogue samples, a three-dimensional (3D)-printed plastic tool was utilised. The spiral scrolls on the shoulders were inscribed in a direction (clockwise when viewed from above) to provide mixing and inwards circulation to pump material towards the centre and avoids mass spilling during the advancing movement. For a rigid engagement of the tool and the substrate, a compression ratio of 3.75% (the difference between the distance of the shoulders and the thickness of the workpiece plates) was used. This is known to induce a better joint for this grade of aluminium.

The BFSW process comparison was conducted on a workpiece of 6 mm thick AA6082-T6 aluminium plates, and multi-layered plasticine slabs of 10 mm thick. Plasticine slabs with thicknesses below 10 mm suffered from instability during the stirring, hence the increase in the thickness of the plasticine samples. Moreover, to guarantee enough material preservation, also to prevent slumping under the shoulders, for plasticine samples the working temperature was lower (0 °C), compared to the aluminium plates (room temperature, 18 °C).

To evaluate the flow features within the weld structure, a variety of speeds -rotational speed; ω (rpm) and advancing speed; V (mm/min)- were applied to produce different flow regimes based on the tool-substrate interaction.

The welding speed sets were initially selected according to previous results for successful BFSW welds of aluminium, see [1,10–12,14,20,27]. For aluminium plates, after running trials, the set of speeds of V (300 and 400 mm/min) and ω (650, 800 and 1000 RPM) were performed to obtain welds with no failure or material loss through the weld-line. However, although the speed sets were able to create a bonded weld, some partial defects were observed which can affect the weld quality.

However when it came to plasticine it was found that these same speeds were unsuitable for making a successful bond, and caused extensive defects and fast rupture in the plasticine samples. Instead it was necessary to go to much slower speeds. These speeds were determined by trial and error, with the criterion being the production of bonded joints. We found a suitable set of speeds for analogue plasticine samples was V (40 and 50 mm/min) and ω (50, 75 and 90 RPM), just above the slowest available speed of the milling machine.

The weld setup comprised the following: the substrate was laid flat in a butt-interface position, with no gap between at the joint line. The tool entered the plate from the locus of the butt-interface. Viewed from behind the tool, the centre of the tool was aligned to the intersection of the workpieces, while the shoulders were evenly in contact with both the top and bottom surfaces of the plate. The tool rotation was clockwise from the top. This means that the advancing side (AS) was situated on the left, and the retreating side (RS) is on the right of the tool, both in the surface plane and cross-sections of the weld-line.

The plasticine weld tests were run using a manual milling machine (MX-45VAE Model, OKUMA brand, Nagoya, Japan). The aluminium weld trials were performed on a 3-axis CNC machining centre (2000 Richmond VMC Model, 600 Group brand, Sydney, Australia) with a 14-horsepower spindle motor capacity. Figure 2 shows the operational details of the BFSW process for the plasticine analogue. For both sets of samples, the bobbin tool had a clockwise rotation viewed from above. To ensure no lateral movement during the BFSW process, the samples were rigidly fixed by the clamp bars in the fixture, with no gaps between the AS and RS workpieces. More details of the BFSW (tool, samples, welding parameters), compared to the aluminium and plasticine tests, are listed in Table 1.

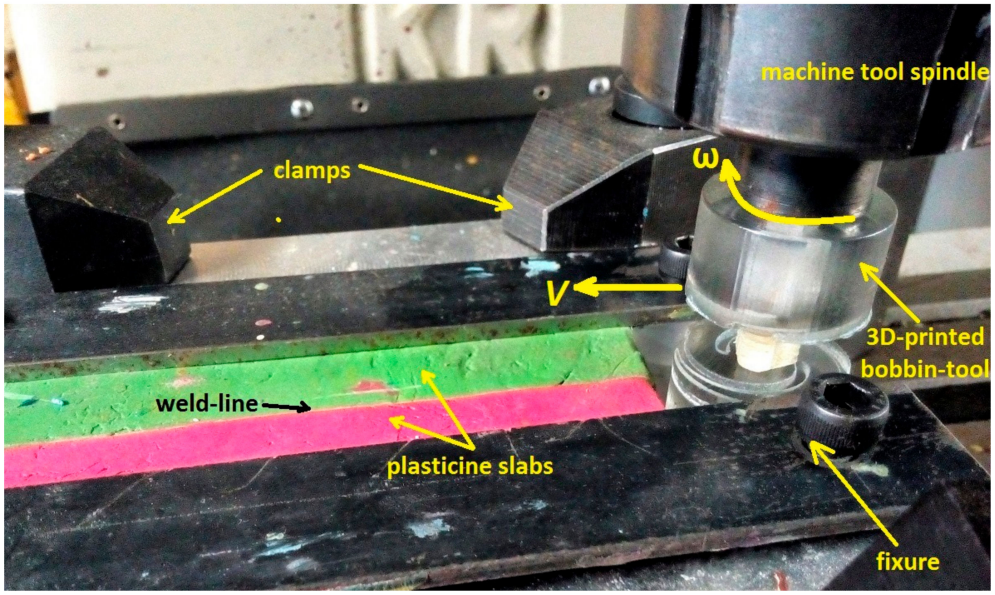

Figure 2. The operational details of the bobbin friction stir welding (BFSW) process for the plasticine analogue.

Table 1. The operational details of the BFSW process for the aluminium and plasticine samples.

Workpiece	Tool Material	$D_{Shoulder}$ (mm)	D_{Pin} (mm)	Plate Thickness (mm)	Feed ω (RPM)	Speed V (mm/min)	Thread Pitch (mm)	Number of Threads
AA6082-T6	H13 Tool Steel	25	5	6	650, 800, 1000	300, 400	1.2	5
Multilayered Plasticine	VeroClear plastic	30	6	10	50, 75, 90	40, 50	1.43	7

After performing a 150 mm single-pass weld-line, the samples were cross-sectioned perpendicular to the welding direction to produce the specimens for the metallographic analysis and flow visualization.

The flow patterns in plasticine analogue samples were observed by a high-resolution bridge digital camera (FinePix S9500 Model, Fujifilm brand, Tokyo, Japan). The digital photographs were recorded under a fluorescent lamp to avoid any shadows in pictures.

The AA6082-T6 weld cross-sections were ground and polished by a standard mechanical polishing to obtain a mirror surface with roughness below 1 µm. To show the metallographic details of the weld, the cross-section specimens were then etched by a reagent solution with the chemical composition of (0.5 g $(NH_4)2MoO_4$ + 3.0 g NH_4Cl + 1 mL HF + 18 mL HNO_3 + 80 mL H_2O). The etching was done by direct immersion of the surface samples in an ultrasonic bath for 90 s, at 70 °C. After washing the samples and drying under hot air, the cross-sections of the aluminium welds were observed by a stereo microscope to show the material flow details.

The plasticine was processed by sectioning with a blade, followed by inspection using the same stereo microscope.

3. Results

3.1. Similarities in Entry Geometry

The plasticine sheets were subject to bobbin friction stir welding (BFSW), and produced identical structural anatomy to aluminium, where similar features were observed regarding the size and shape of the patterns, see Figures 3 and 4. For the beginning of the weld, these include the entry spray on the retreating side (RS), and a channel discontinuity on the advancing side (AS) which is representative of the tunnel void. Note, the relative sizes of these two sprays in analogue and aluminium welds are approximately the same. As the clockwise-rotating tool enters the substrate, it ejects material into the air at its rear and onto the retreating side. Hence, the large spray at the entry location protruded to the RS. A smaller amount of material is picked up by the tool and transferred to the advancing side (see Figure 4). Note also, the similarity of the surface patterns. This is characterized by a shredded appearance, which is attributed to the threads and flats on the tool. These features are the same in both materials. Likewise the tunnel defect, both its location (underside), laterally deflected to the advancing side, and its granular internal surface is the same.

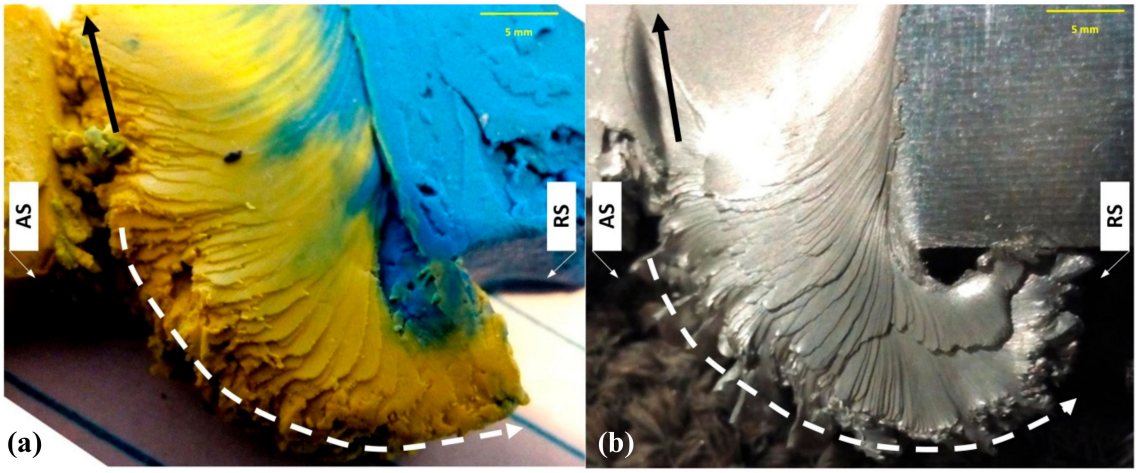

Figure 3. Macroscopic structural features of entry-zone sprayed tail, produced via bobbin friction stir welding, (**a**) plasticine (50 rpm, 50 mm/min) and (**b**) aluminium 6082-T6 (650 rpm, 400 mm/min), in both cases. The Figure shows the top-view.

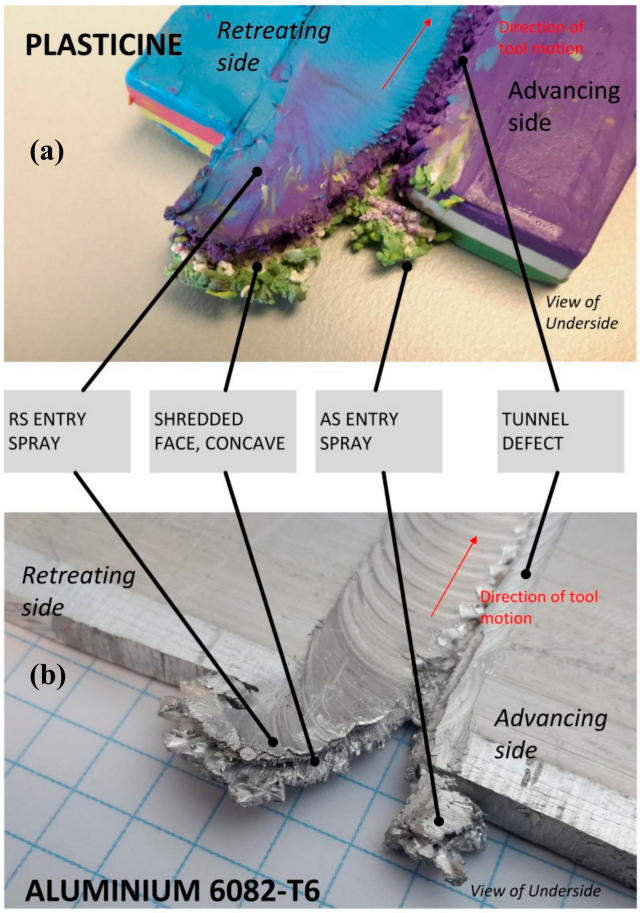

Figure 4. Macroscopic structural features of bobbin friction stir welding, (**a**) plasticine slab (75 rpm, 50 mm/min), and (**b**) AA6082-T6 aluminium plate (650 rpm, 400 mm/min). In both cases, the rotation is clockwise when viewed from above, although, this view is from below. Figure shows the common features. Image adapted from Tamadon et al., *Metals*; published by MDPI, 2018 [14].

It is concluded that the plasticine faithfully represents the structural anatomy of BFSW in aluminium. The analogue methodology, therefore, has the potential to explore flow behaviours in

BFSW. The capability of the plasticine analogue to produce the geometric features of the BFSW weld makes it a suitable candidate to be used for analogue modelling of BFSW.

3.2. Weld Surface under the Shoulder

To understand the flow mechanism induced by the shoulder, the weld surface can be an initial place for observations, as it is readily observable without destructive tests. The overall surface flow at the surface field pitch is demonstrated for aluminium and plasticine samples in Figure 5.

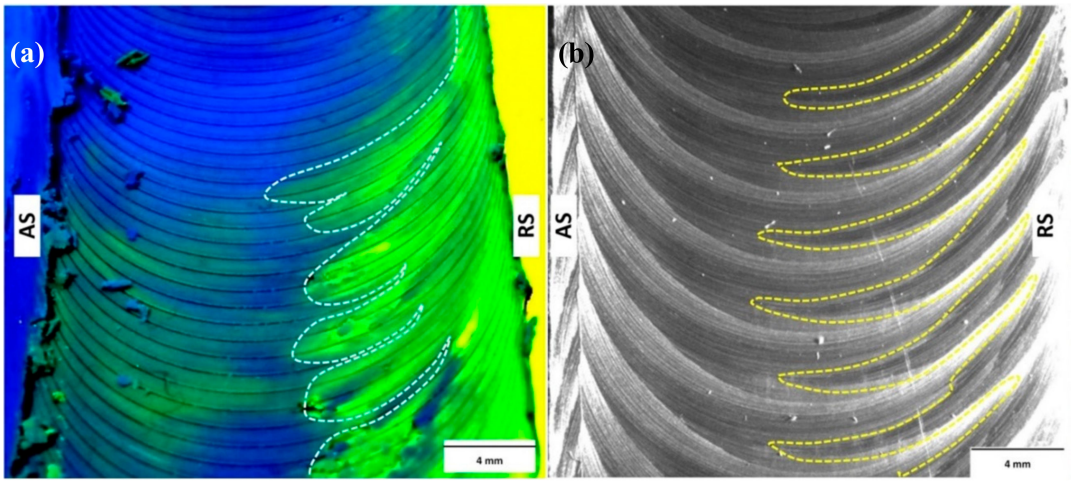

Figure 5. Surface flow patterns of the BFSW weld samples; (**a**) plasticine (50 rpm, 50 mm/min), and (**b**) aluminium 6082-T6 (650 rpm, 400 mm/min). In both cases figures show the top-view.

The typical surface appearance of the FSW weld is a periodic pattern of the circular ripples, pitched towards the initial starting position of the tool rotation. These surface weld pitches are a direct outcome of the shoulder action at the surface of the workpiece, formed by the material deposition at the rear circumferential of the shoulder (trailing edge of the tool). By the advancement of the tool, the stirred massed at the leading edge of the tool undergoes traverse transportation between the AS and RS of the weld section.

The combined relative motion of the tool (rotating and advancing) is responsible for this ripple pattern by a successive revolution and overlapping between the deposited pitch layers. The thickness of the pitch layers is defined as the distance per revolution, which is related to the speed ratio of the FSW tool (V/ω) or (mm/RPM).

To understand the overall planar flow, a comparison between the aluminium weld surface and the analogous plasticine sample is shown in Figure 5. For both samples, the effect of the shoulder action on the weld surface is related to the speed ratio (distance/rev).

The surface flow visualization shows a flow patch pattern at the RS edge of the weld. Our interpretation attributes this feature to the lateral revolution of the tool after deposition of the mass layers at the trailing edge, with a simultaneous forward movement which induces an opposite flow between the direction of V and ω at the rear edge of whereby an aluminium weld sample, with intensified flow patch patterns at the RS, is compared with the colour-layered plasticine model, (see Figure 6a–d). The plasticine results are given for three different regions, all sectioned at 1 mm below the surface and viewed in plane view. Both samples experienced similar flow patterns at the RS vicinity of the shoulder. The plasticine results reveal that the turbulent flow extends to below the surface, and not merely due to a superficial effect.

Also, these flows appear to be associated with the formation of a tunnel defect discontinuity in the stirring zone (SZ) on the side towards the AS. The flow distribution during the material mixing can provoke a macro-scale discontinuity defect in the weld. The horizontal section shows the circular shape of the material flow patterns. These were deposited at the trailing edge of the shoulder.

While, the clockwise rotating tool moves forward, it causes a bending direction for the backward accumulated layers by a transverse extruding towards the advancing side. A further understanding of the shoulder-tool flow interaction requires consideration of the cross-sections.

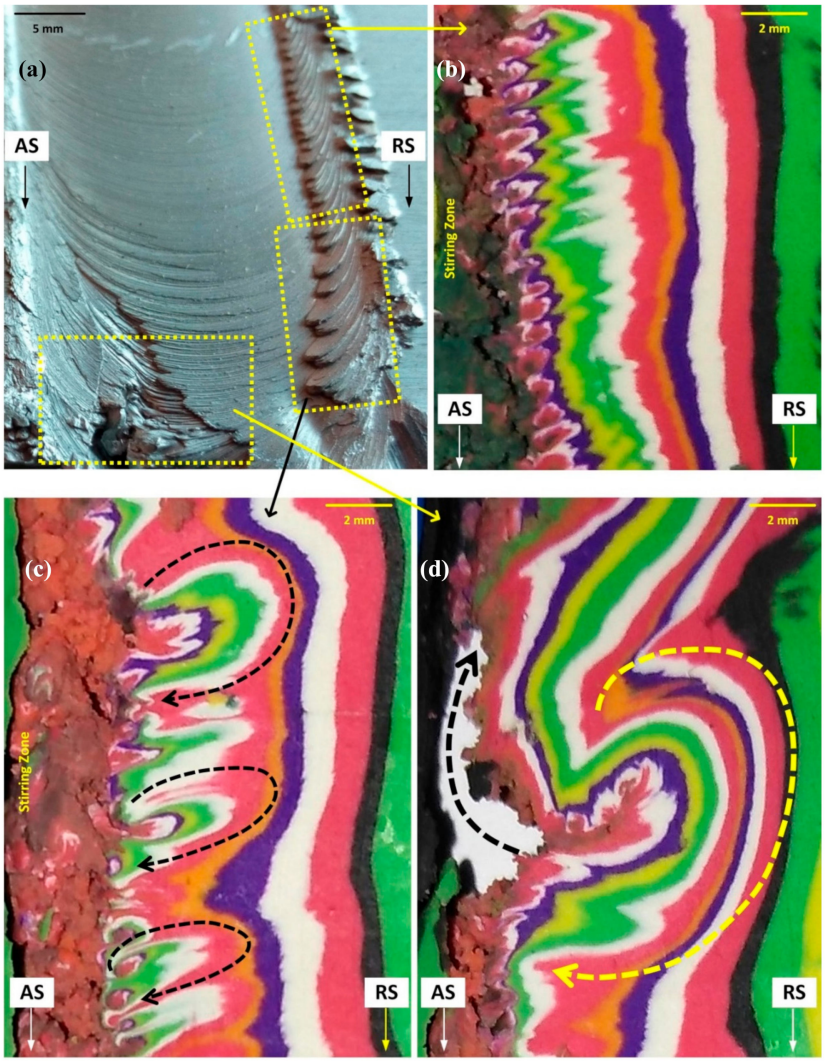

Figure 6. Surface flow patterns of the BFSW weld samples on (**a**) aluminium 6082-T6 (650 rpm, 400 mm/min), and (**b**–**d**) plasticine analogue (50 rpm, 50 mm/min), top views. The plasticine results are given for three different regions, all sectioned at 1 mm below the surface.

3.3. Cross Sections

3.3.1. Macroscopic Features across the Weld as a Whole

The difference of the flow patterns through the weld cross-section can reveal the material transportation mechanism between the AS and the RS during the stirring action. This is only evident in the plasticine case, as the aluminium cannot realistically be etched in any way to show this. Hence, this analogue model has the potential to be used to infer flow processes that are not visible in aluminium. Figure 7 shows the comparison of the internal flow features within the transverse sections of the plasticine analogue and aluminium weld samples. The samples were cross-sectioned perpendicular to the welding advancement direction.

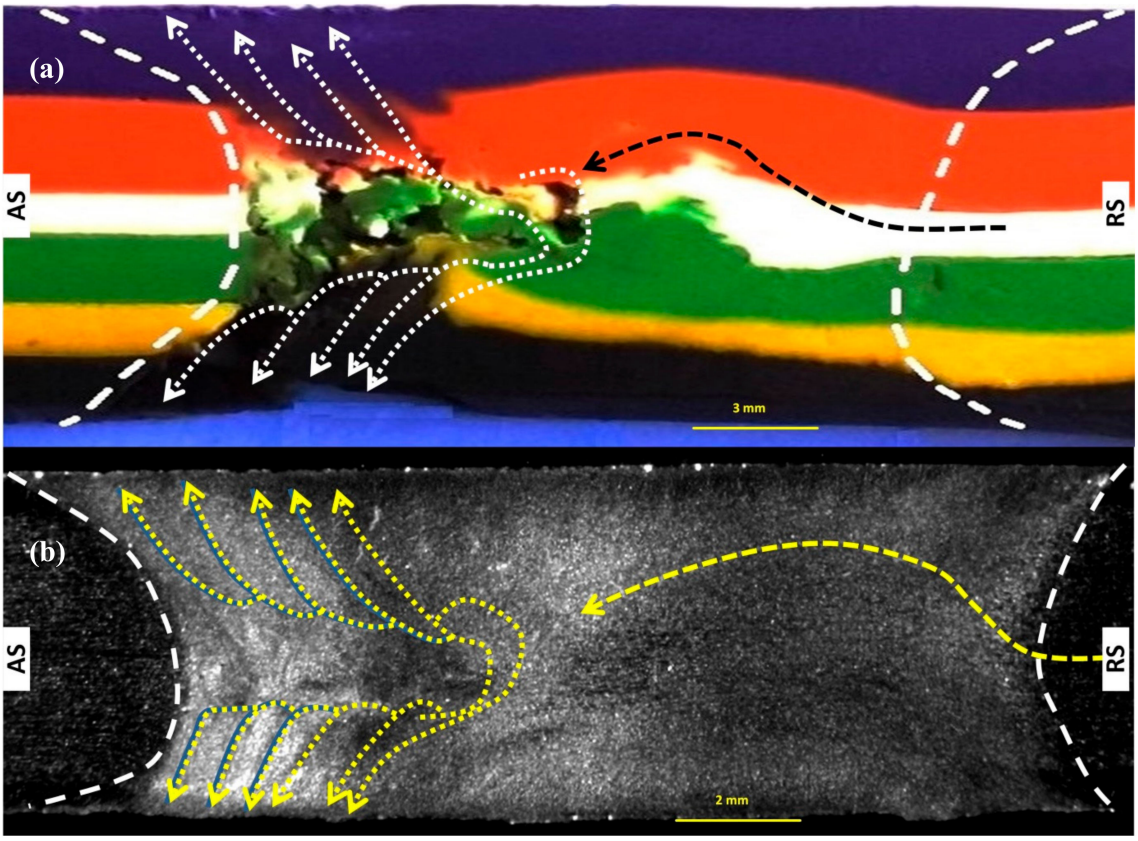

Figure 7. Cross-section of the BFSW weld, (**a**) plasticine sample (50 rpm, 50 mm/min), and (**b**) aluminium weld (650 rpm, 400 mm/min).

As a general comment on the weld flow, there is a common characteristic as the flow layers are severely distorted on the advancing side border compared to the retreating side. Consequently, the mixing of the material is preferentially localized towards the AS. This can be due to the stronger shearing action in the AS proximity of the rotating tool. The uniformity of the mass flow is poor at the AS, with flow going in different directions at the deposition stage. This likely contributes to the formation of the tunnel void at this location, rather than centrally or at the RS.

Another interesting flow feature, which can be visualized by the analogue model, is the sub-shoulder flow pattern. This shows an independent flow behaviour compared to the deeper region, which is affected by the pin performance. Although, some flow features are visible in Figure 7a, the effects are more apparent at higher welding speeds, where the flow dispersion is increased by the intensified shearing.

In Figure 8, the tunnel defect is observed for both analogue plasticine and aluminium welds. Insufficient material mixing limits the integrity of flow during the mass transportation behind the tool. In this situation, the downward flow (towards the bottom of the AS) is reduced, causing refilling failure problems at the bottom part of the cross-section, hence contributing to the tunnel defect. Note also that the plasticine shows the upper layers as being serrated but still intact, whereas the lower layers are shredded and suffer from poor compaction mid-substrate. By analogy, the tunnel void in the aluminum would then also be a compaction issue. The presumed upwards helical flow of material, due to the threads, is expected to be another factor.

The plasticine also elucidates the flow in the region from the middle of the stirring zone towards the RS. A notable feature is the bulged or blip-shaped expansion of the flow layers, most readily apparent in the pink layer of Figure 8b. A possible explanation of this flow feature is as follows. Shearing of the material flow at the sub-shoulder regions induces a continuous vortex-like flow. Simultaneously the pin motion induces another vortex in the mid-SZ. By the rotational and advancing movement of the

pin, this pushes the material to the leading edge of the tool at the AS and pulls the mass from the RS into the trailing edge of the tool. During this process the central layers are not treated equally.

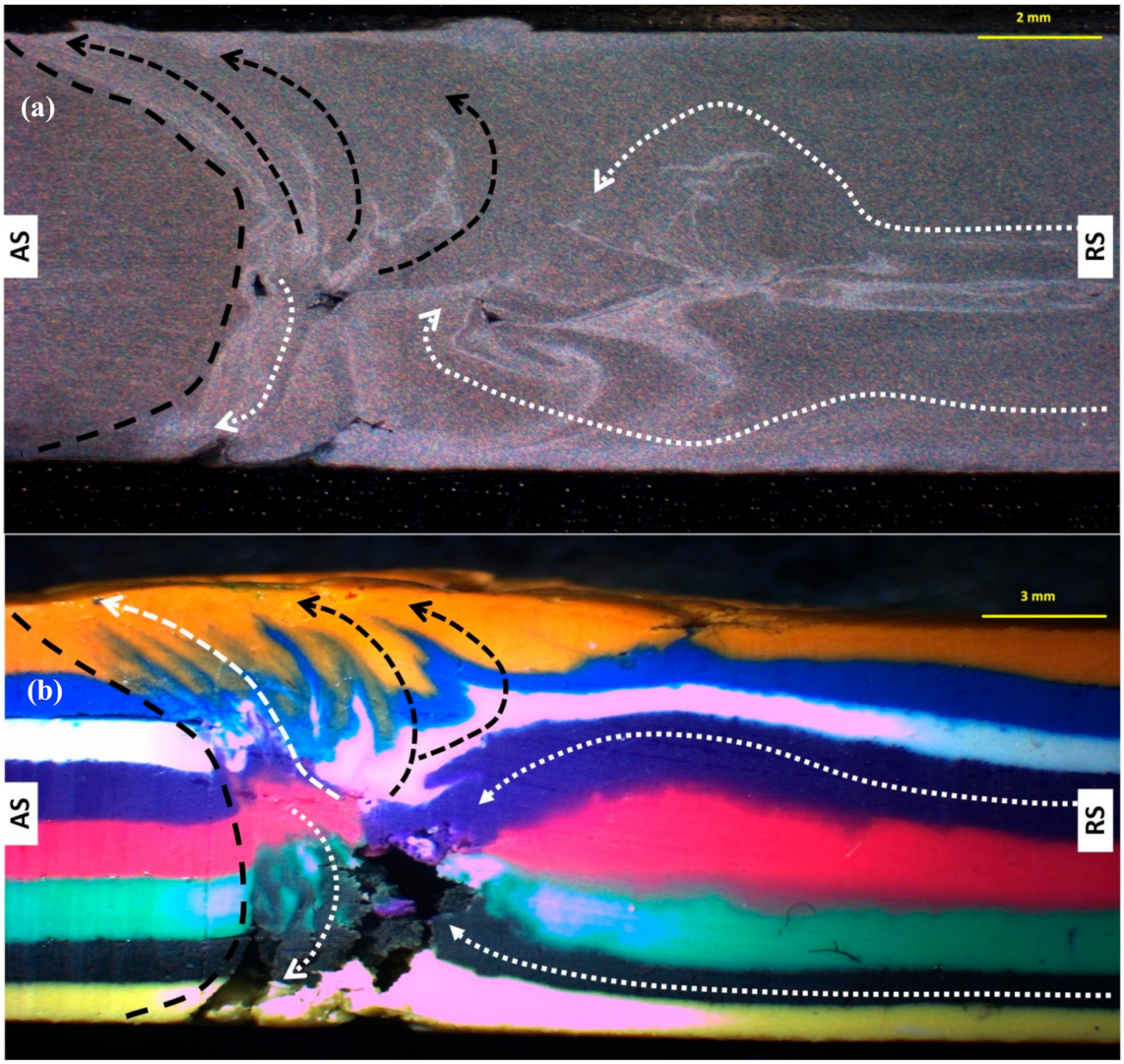

Figure 8. Joint sections; (**a**) aluminium sample (800 rpm, 400 mm/min), and (**b**) plasticine analogue (75 rpm, 50 mm/min).

Figures 9–11 compare the weld cross-sections for different welding speeds (ω, V). Also, using bi-colour plasticine slabs, with different colours on the AS and RS plates, allows the transfer of material across the joint to be revealed in greater detail, something which is impractical to achieve in the aluminium weld samples.

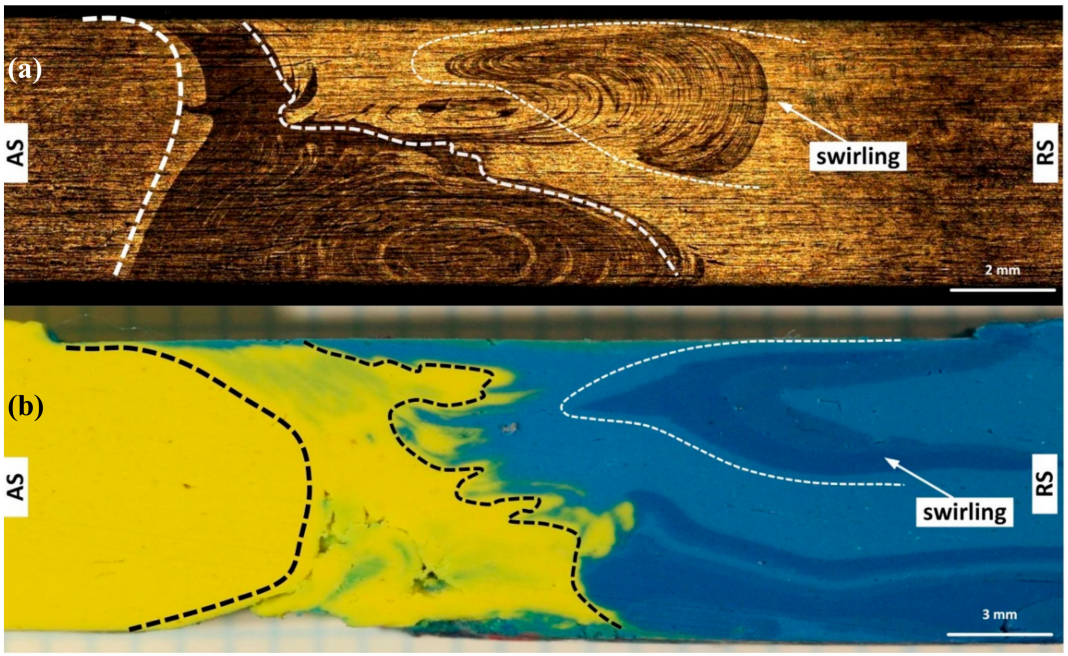

Figure 9. Swirling pattern at the mid-thickness cross-section of the weld, the jugged intermixing at the mid-stirring zone, representative of the shear layers around the pin, situated between top and bottom shoulders; (**a**) aluminium sample (1000 rpm, 300 mm/min), and (**b**) bi-colour plasticine analogue (90 rpm, 40 mm/min).

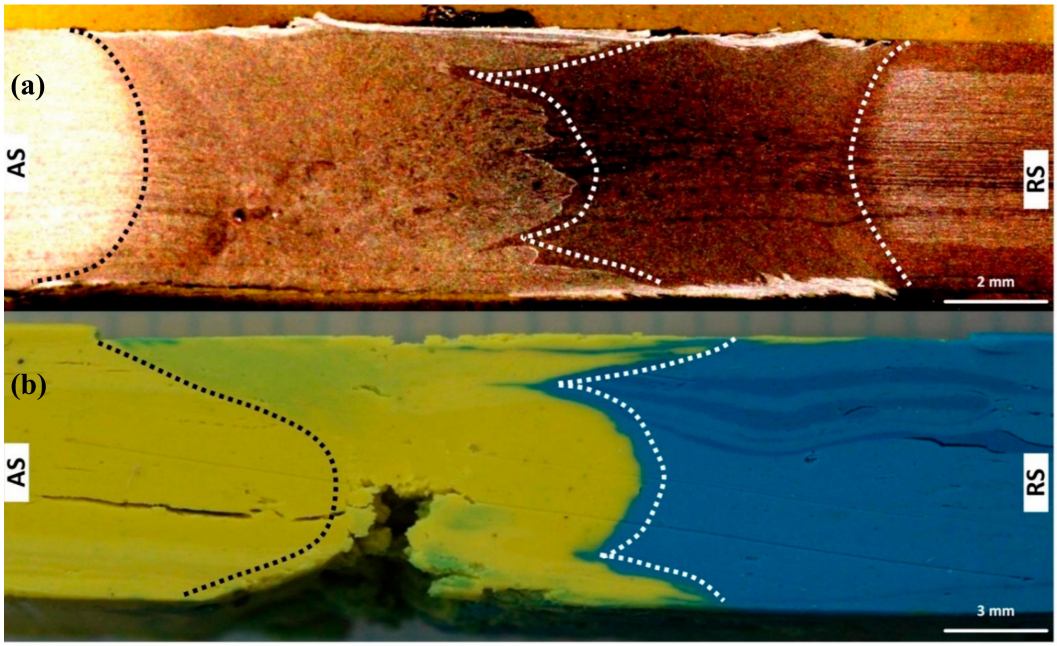

Figure 10. Elliptical mixed pattern at the mid-thickness pattern, pulled upward and downward, repeated along AS-to-RS; (**a**) aluminium sample (1000 rpm, 400 mm/min), and (**b**) bi-colour plasticine analogue (90 rpm, 50 mm/min).

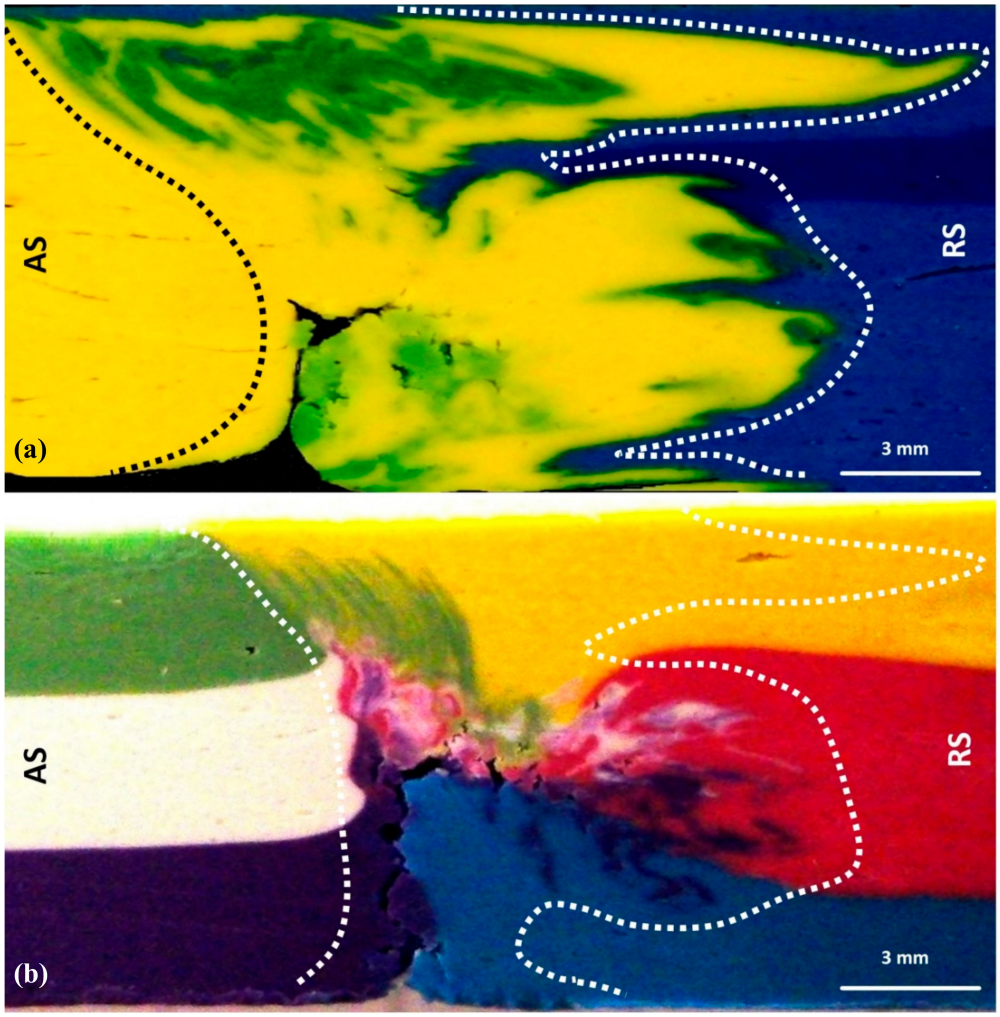

Figure 11. Mixed layers, showing flow lines under the shoulder; (**a**) bi-colour plasticine slab (75 rpm, 40 mm/min), and (**b**) multi-coloured plasticine slab (90 rpm, 50 mm/min).

In all the stirring conditions, it was noticeable in the plasticine that there are small localized regions of well-mixed material, particularly at the top of the AS. However, in general, the material flow had penetrated from the AS into RS.

Figure 9, for the plasticine analogue, shows a mixing region underneath the top shoulder, which is consistent with the aluminium weld. Similar to this flow feature, a narrow mixed area is also observed near the bottom shoulder.

Regarding the welding speeds, it should be noted that the elevated RPM has a more significant role in the stirring action, compared to the travelling speed. Hence, the material around the rotating pin and underneath the shoulders may undergo multiple circulations while travelling forward. This increases the mixing rate during stirring. In this condition, if the feed rate during the forward motion does not properly support the flow around the pin, the integrity of the flow can be adversely affected.

An elliptical mixing pattern is evident, Figure 10. Our interpretation is that at higher rotational speeds, the sub-shoulder regions induce more flow and large-scale mixing into the SZ, and the pin entrains a larger volume of stirred material, hence, forming the shapes observed.

3.3.2. Mixing under the Shoulder

There is a thin surface layer that is smeared over the top and bottom surfaces. The plasticine identifies that this is an approximately equal mix of material from the advancing and retreating sides. This is most evident in Figure 11. This is consistent with the widely-accepted function of the shoulder. There is a deeper mixing under the shoulder, which appears on the AS upper region only. This comprises multiple jagged flow arms. The plasticine shows this comprises layered fragments of the AS material (upper layer). What is interesting in Figure 11b, is that the narrowness of these flow-arm layers, in the aluminium, is faithfully reproduced in the plasticine.

In Figure 11, the sub-shoulder flow patterns have been visualized in the cross-section of the weld. The narrow flow layers are attributed to packets of material formed at the interface of the threads-flats that are moved around the pin from AS to RS, and then deposited and packed up against the AS trailing edge of the pin. The consolidation explanation is consistent with the observation that the lower regions of the AS, either have flow layers or tunnel defect, not both.

A remaining question remains about the nature of the flow arms. Our interpretation is that the actual direction of flow in these features is shear perpendicular to the cross-section plane (towards and away from the line of sight) and an element of compression orthogonal to the arms (in plane). Different cross-sectioning of the weld samples, parallel to the weld-line direction, might be useful to find more details of the flow lines.

The clockwise direction of the tool rotation causes an asymmetric material flow circulation through the stirring zone. This causes the plastic flow to be dispersed in different directions at the proximity of the tool, where the mass layers undergo different levels of deformation and intermixing. During the tool-workpiece interaction, fragments of the plasticized mass are transported in a circulating pathway around the tool, starting from the leading edge, undergo a chaotic flow, and are squeezed to the trailing edge where they are deposited in the weld-seam. At the trailing edge, the flow packets are dispersed into the RS layers to migrate across the centre-line of the weld section, eventually to settle at the AS hourglass-border. However, loss of material at entry creates a deficit in the cross sectional area, which impedes the compaction process, hence the AS border wall is where the flow discontinuity is most likely to occur.

4. Discussion

4.1. Summary of Outcomes

The analogue model showed the tool performance causing a variety of flow patterns associated with discontinuity defects through the structure of the weld. Excellent mixing was observed in localized areas, which comprised intercalated regimes corresponding to solid-state bonding. The use of multi-coloured layers of plasticine provides valuable insights into the otherwise invisible plastic flow mechanisms in aluminium BFSW as a solid-state joining process.

The plastic deformation pattern shows a turbulent flow around the tunnel void defect. The cascading shape of the plastic flow arms at the hourglass-border can be attributed to the shear stress field introduced by the pin and intensified at the sub-shoulder region. The jagged features in the tunnel defect are attributed to shear bands emerging from failure of the material flow. This has been shown in Figure 12 for the macro-etched cross-sections of the weld, for the similar welding conditions with, and without, the emergence of the defect.

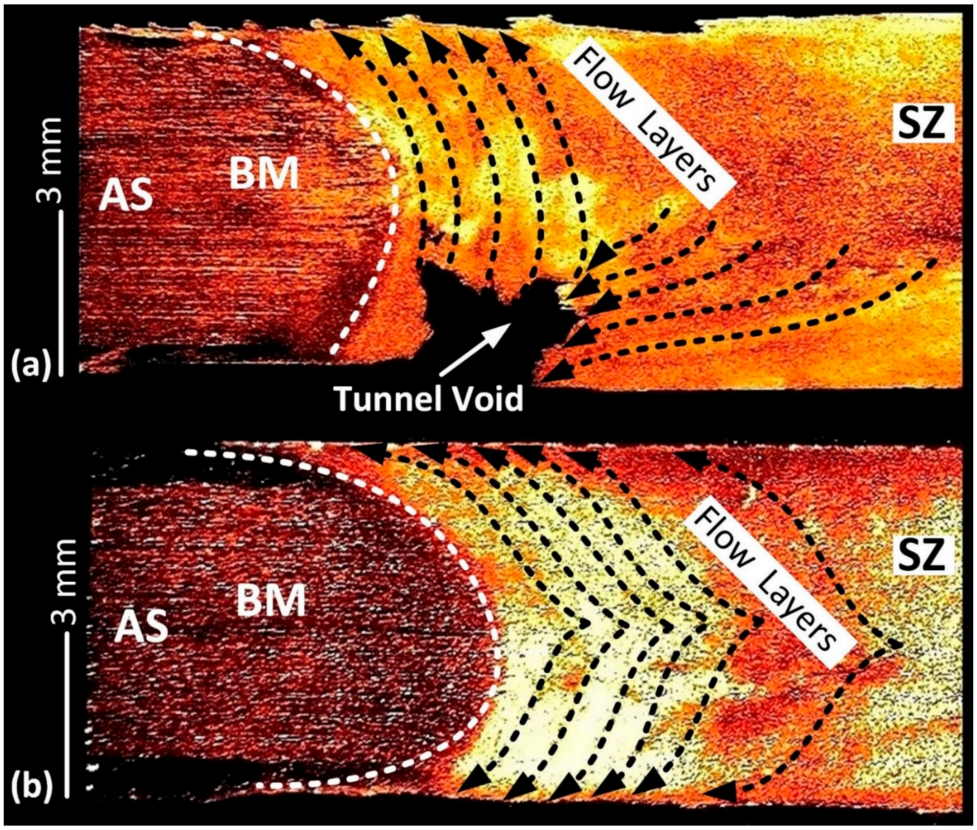

Figure 12. The proposed flow patterns at the AS location of the stirring zone, drawn at the weld cross-section; (**a**) in presence of the tunnel void (w = 400 rpm, 350 mm/min), and (**b**) for a defect-free sample (w = 650 rpm, 400 mm/min). Image adapted from Tamadon et al., *Metals*; published by MDPI, 2019 [1].

The defect-free weld (Figure 12b) possesses uniform flow lines, that are dispersed from the weld centre (at the position of the tool) towards the AS border. Because of the forging effect of the rotating shoulders, the flow lines are directed towards the top and bottom shoulders. This forms a bent-shaped hourglass border at the boundaries of the stirring zone. In Figure 12a, the failure of the flow regimes leads to dispersion of the flow lines from the centre of the weld towards the AS border. Therefore, the un-bonded layers of the deposited mass form the open tunnel void. The tunnel defect is representative of the continuous discontinuity at the bottom side of the AS weld region [27].

4.2. Towards a Model of the Formation of the Tunnel Void

There is no solid theory regarding the flow-based mechanism of the tunnel void formation, hence, we provide some interpretations based on observation of the plasticine analogue.

Figure 13 shows a physical model for the occurrence of the tunnel void, based on the flow-based approach applied in analogue modelling. The picture of the actual void at the beginning of the formation at the entry zone of the weldment is shown in Figure 13a. It suggests that the flow lines during the transportation from the RS to AS and deposition at the trailing edge of the tool, are deviated by the sub-shoulder flow effect. This stretches the flow lines upwards and downwards, thereby, deteriorating the integrity of the refilling of the stirred layers, and hence causing an un-bonded discontinuity at the AS border.

Figure 13b provides a general schematic of the flow regimes at the stirring zone of the BFSW process, where the flow patches at the proximity of the pin begin to form the plasticized mass until finally they are deposited at the back of the tool and form an hourglass-shaped stirred zone at the cross-section of the weld.

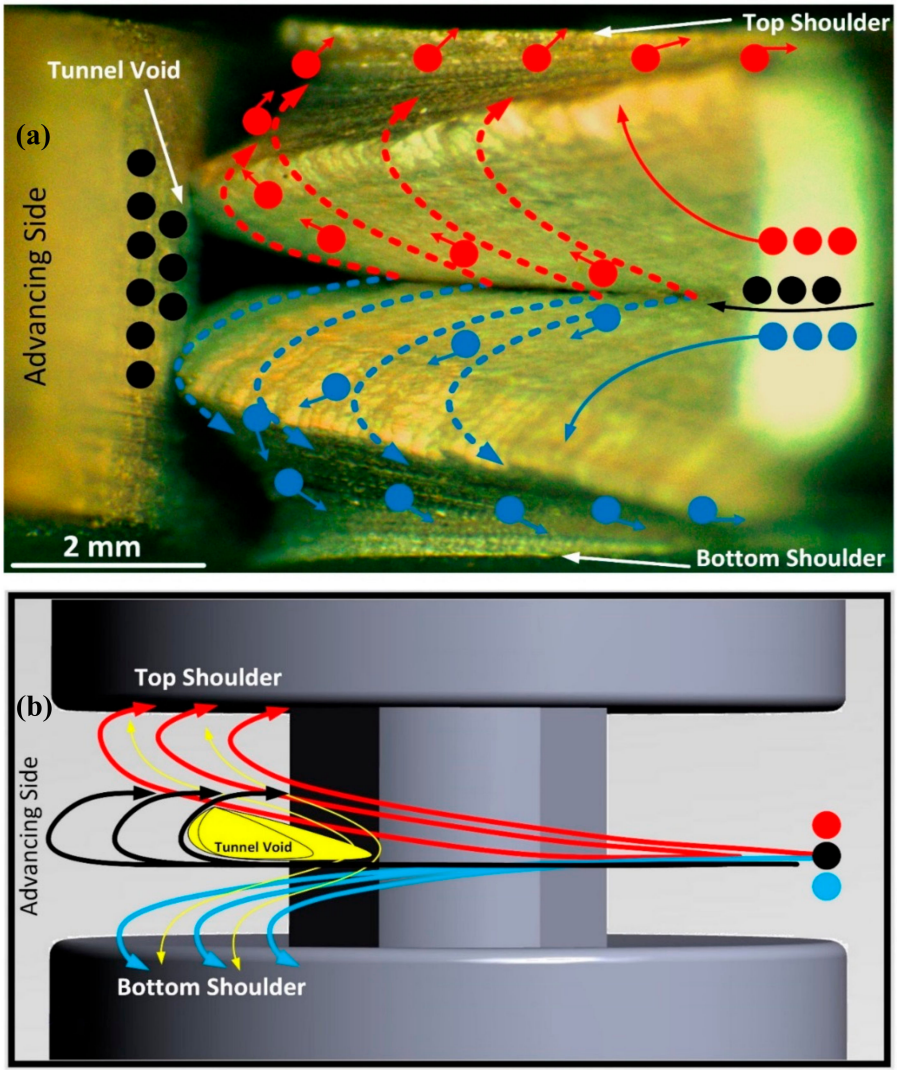

Figure 13. The proposed flow model for the formation of the tunnel void at the AS location of the stirring zone; (**a**) physical model at the position of the tunnel void, (**b**) schematic of the proposed model for the formation of the tunnel void within the flow lines around the rotating pin.

Based on the visualisation of the flow layers at the cross-section of the weld, we suggest that the reduced integrity of material flow and the decreased consolidation cause the tunnel void at the AS position of the weld. The tunnel defect occurs at the AS because this is the last region for the deposition of material at the trailing edge of the tool. The tunnel occurs at the bottom because the threads on the pin pump the flow upwards. The tunnel is further intensified by the loss of material from the cross-section, where this loss primarily occurs at the edge entry.

4.3. Implications for Future Work

There is an interesting question as to whether there is a principle of dynamic similitude that might apply, and what the process might be for obtaining the feed and speed parameters. There are no known principles of similitude for this particular situation, and some reason to believe [28,29] that it is impossible to scale all features of metal forming processes in general. If it was possible to develop a similitude approach to analogue modelling of BFSW, it would seem to require the development of a transport equation, perhaps along the lines envisaged by [28,29] (where the scaling factors for press forming were volume, mass, momentum, movement, energy, and others). In a forging process the geometry dominates the final shape, somewhat irrespective of all other factors. In contrast the BFSW

situation is expected to be more complex because, not only is there a geometry constraint imposed by the tool, but also a dynamic flow component, with the opportunity for material to escape (e.g., at entry). Possible variables to consider might be the coefficient of friction, mechanical strength, and material stiffness. This is left for future work.

5. Conclusions

The flow behaviour during bobbin friction stir welding was visualized using a plasticine analogue, and compared to aluminium welds. The weld tests demonstrated the surface and internal flow features obtained from the interaction between the rotating tool and the substrate. The transverse transportation of the plastic flow, between the retreating and advancing sides, creates a mass refilling mechanism as a result of the stirring action. The failure of this flow appears to cause tunnel void discontinuity. A flow-based model was proposed for the formation mechanism of the tunnel void at the trailing edge of the tool near the advancing side of the weld seam.

Author Contributions: Conceptualization, A.T. and D.J.P.; methodology, A.T.; validation, A.T.; formal analysis, A.T. and D.J.P.; writing—original draft preparation, A.T.; writing—review and editing, A.T., D.J.P., and D.C.; supervision, D.J.P. and D.C. All authors have read and agreed to the published version of the manuscript.

Funding: This research received no external funding.

Conflicts of Interest: The authors declare no conflict of interest.

References

1. Tamadon, A.; Pons, D.J.; Clucas, D.; Sued, K. Internal Material Flow Layers in AA6082-T6 Butt-Joints during Bobbin Friction Stir Welding. *Metals* **2019**, *9*, 1059. [CrossRef]
2. Thomas, W.; Wiesner, C.; Marks, D.; Staines, D. Conventional and bobbin friction stir welding of 12% chromium alloy steel using composite refractory tool materials. *Sci. Technol. Weld. Join.* **2009**, *14*, 247–253. [CrossRef]
3. Threadgill, P.L.; Ahmed, M.; Martin, J.P.; Perrett, J.G.; Wynne, B.P. The use of bobbin tools for friction stir welding of aluminium alloys. *Mater. Sci. Forum* **2010**, *638*, 1179–1184. [CrossRef]
4. Thomas, W.; Nicholas, E. Friction stir welding for the transportation industries. *Mater. Des.* **1997**, *18*, 269–273. [CrossRef]
5. Thomas, W.; Nicholas, E.; Needham, J.; Murch, M.; Temple-Smith, P.; Dawes, C. Friction Stir Butt Welding. International Patent Application No. Pct/Gb92 Patent Application No. 9125978.8, 6 December 1991.
6. Sued, M.K. Fixed Bobbin Friction Stir Welding of Marine Grade Aluminium. Ph.D. Thesis, University of Canterbury, Christchurch, New Zealand, April 2015.
7. Threadgill, P.; Leonard, A.; Shercliff, H.; Withers, P. Friction stir welding of aluminium alloys. *Int. Mater. Rev.* **2009**, *54*, 49–93. [CrossRef]
8. Hilgert, J.; Schmidt, H.; Dos Santos, J.; Huber, N. Thermal models for bobbin tool friction stir welding. *J. Mater. Process. Technol.* **2011**, *211*, 197–204. [CrossRef]
9. Hilgert, J.; Hütsch, L.L.; dos Santos, J.; Huber, N. Material Flow around a Bobbin Tool for Friction Stir Welding. Excerpt from the Proceedings of the COMSOL Conference. 2010. Available online: https://cds.comsol.com/paper/download/63672/hilgert_paper.pdf?__gda__=1579495574_5ad8b2c54042c8a4c775cf836ec9714b&fileExt=.pdf (accessed on 20 January 2020).
10. Sued, M.; Pons, D.; Lavroff, J.; Wong, E.-H. Design features for bobbin friction stir welding tools: Development of a conceptual model linking the underlying physics to the production process. *Mater. Des. (1980–2015)* **2014**, *54*, 632–643. [CrossRef]
11. Tamadon, A.; Pons, D.; Sued, M.; Clucas, D.; Wong, E. Analogue modelling of bobbin tool friction stir welding. In Proceedings of the International Conference on Innovative Design and Manufacturing (ICIDM2016), Auckland, New Zealand, 24–26 January 2016.
12. Sued, M.; Tamadon, A.; Pons, D. Material flow visualization in bobbin friction stir welding by analogue model. *Proc. Mech. Eng. Res. Day* **2017**, *2017*, 1–2.

13. Tamadon, A.; Pons, D.; Sued, M.; Clucas, D.; Wong, E. Preparation of Plasticine Material for Analogue Modelling. In Proceedings of the International Conference on Innovative Design and Manufacturing (ICIDM2016), Auckland, New Zealand, 24–26 January 2016.
14. Tamadon, A.; Pons, D.; Sued, K.; Clucas, D. Formation mechanisms for entry and exit defects in bobbin friction stir welding. *Metals* **2018**, *8*, 33. [CrossRef]
15. Gadakh, V.S.; Adepu, K. Heat generation model for taper cylindrical pin profile in FSW. *J. Mater. Res. Technol.* **2013**, *2*, 370–375. [CrossRef]
16. Dong, P.; Dou, Z.; Zhang, P. 3D numerical simulation of temperature and stress evolution in friction stir welding of aluminum alloy. *Hanjie Xuebao* **2015**, *36*, 71–74.
17. Fonda, R.; Reynolds, A.; Feng, C.; Knipling, K.; Rowenhorst, D. Material flow in friction stir welds. *Metall. Mater. Trans. A* **2013**, *44*, 337–344. [CrossRef]
18. Fuse, K.; Badheka, V. Bobbin tool friction stir welding: A review. *Sci. Technol. Weld. Join.* **2019**, *24*, 277–304. [CrossRef]
19. Hasan, A.F.; Bennett, C.J.; Shipway, P.H. A numerical comparison of the flow behaviour in Friction Stir Welding (FSW) using unworn and worn tool geometries. *Mater. Des.* **2015**. [CrossRef]
20. Tamadon, A.; Pons, D.; Sued, K.; Clucas, D. Development of metallographic etchants for the microstructure evolution of A6082-T6 BFSW welds. *Metals* **2017**, *7*, 423. [CrossRef]
21. Dialami, N.; Cervera, M.; Chiumenti, M. Effect of the tool tilt angle on the heat generation and the material flow in friction stir welding. *Metals* **2019**, *9*, 28. [CrossRef]
22. Abdel Wahab, M. Editorial: Applied Mechanics. *Appl. Mech.* **2020**, *1*, 1–2. [CrossRef]
23. Tayon, W.A.; Domack, M.S.; Hoffman, E.K.; Hales, S.J. Texture evolution within the thermomechanically affected zone of an Al-Li alloy 2195 friction stir weld. *Metall. Mater. Trans. A* **2013**, *44*, 4906–4913. [CrossRef]
24. Tamadon, A.; Pons, D.J.; Clucas, D.; Sued, K. Texture Evolution in AA6082-T6 BFSW Welds: Optical Microscopy and EBSD Characterisation. *Materials* **2019**, *12*, 3215. [CrossRef]
25. Tamadon, A.; Pons, D.; Sued, K.; Clucas, D. Thermomechanical grain refinement in AA6082-T6 thin plates under Bobbin friction stir welding. *Metals* **2018**, *8*, 375. [CrossRef]
26. Tamadon, A.; Pons, D.J.; Clucas, D. AFM Characterization of Stir-Induced Micro-Flow Features within the AA6082-T6 BFSW Welds. *Technologies* **2019**, *7*, 80. [CrossRef]
27. Tamadon, A.; Pons, D.J.; Clucas, D. Structural Anatomy of Tunnel Void Defect in Bobbin Friction Stir Welding, Elucidated by the Analogue Modelling. *Appl. Syst. Innov.* **2020**, *3*, 2. [CrossRef]
28. Krishnamurthy, B.; Bylya, O.; Davey, K. Physical modelling for metal forming processes. *Procedia Eng.* **2017**, *207*, 1075–1080. [CrossRef]
29. Casaburo, A.; Petrone, G.; Franco, F.; De Rosa, S. A Review of Similitude Methods for Structural Engineering. *Appl. Mech. Rev.* **2019**, *71*, 030802. [CrossRef]